



Circulation induced by subglacial discharge in glacial fjords: Results from idealized numerical simulations

Julio Salcedo-Castro^{a,*}, Daniel Bourgault^b, Brad deYoung^a

^a Department of Physics and Physical Oceanography, Memorial University of Newfoundland, St. John's, NL, Canada A1B 3X7

^b Institut des sciences de la mer de Rimouski, Université du Québec à Rimouski, 310 allée des Ursulines, Rimouski, Québec, Canada

ARTICLE INFO

Article history:

Received 31 October 2010

Received in revised form

2 June 2011

Accepted 6 June 2011

Available online 15 June 2011

Keywords:

Glacier

Estuary

Plume

Buoyancy flux

Potential energy anomaly

ABSTRACT

The flow caused by the discharge of freshwater underneath a glacier into an idealized fjord is simulated with a 2D non-hydrostatic model. As the freshwater leaves horizontally the subglacial opening into a fjord of uniformly denser water it spreads along the bottom as a jet, until buoyancy forces it to rise. During the initial rising phase, the plume meanders into complex flow patterns while mixing with the surrounding fluid until it reaches the surface and then spreads horizontally as a surface seaward flowing plume of brackish water. The process induces an estuarine-like circulation. Once steady-state is reached, the flow consists of an almost undiluted buoyant plume rising straight along the face of the glacier that turns into a horizontal surface layer thickening as it flows seaward. Over the range of parameters examined, the estuarine circulation is dynamically unstable with gradient Richardson number at the sheared interface having values of $< 1/4$. The surface velocity and dilution factors are strongly and non-linearly related to the Froude number. It is the buoyancy flux that primarily controls the resulting circulation with the momentum flux playing a secondary role.

© 2011 Elsevier Ltd. All rights reserved.

1. Introduction

Polar regions are particularly sensitive to global climate change since glaciers and ice caps are among the systems that show the most significant response to warming (Solomon et al., 2007). For example, substantial reductions of the sea-ice pack extent may lead to important changes to the structure and function of the Arctic marine environment, such as increases in meltwater outflow (Solomon et al., 2007) and greater sediment input to coastal marine environments (Peizhen et al., 2001).

The connection between ice and ocean boundaries in Arctic environments can be through glacial fjords. In these systems, freshwater can come from supraglacial flows (from melting at the top of glacier), subsurface freshwater discharges which can be at middle depth (englacial) or underneath the glacier (subglacial), or ice melting at the front (submerged and emerged) of the glacier produced by the ambient water. The last process has been proposed as the main mechanism driving the vertical circulation and melt driven upwelling along the glaciers and icebergs face, from a combination of laboratory and theoretical studies (Josberger and Martin, 1981), field observations in the Weddell Sea (Neshyba,

1977), icebergs off NE coast of Newfoundland (Josberger and Neshyba, 1980) and South Cape Fiord (Horne, 1985), and a combination of laboratory and field studies in the Labrador Sea (Josberger, 1978) and the Antarctic (Neshyba and Josberger, 1980).

In some subpolar glacial fjords, however, the glacial ice melting can be masked by the much larger freshwater input from subglacial streams, during the melting season, as observed in Muir Inlet by Matthews and Quinlan (1975) and in Columbia Bay by Walters et al. (1988). The same conclusion was reached by Mackiewicz et al. (1984) in a study of Muir Inlet, and by Cowan (1992), in a study of McBride Inlet. This has also been stated by Svendsen et al. (2002), in their study of the Kongsfjorden–Krossfjorden system, and, more recently, by Motyka et al. (2003), who applied a model for convective flow in proglacial waters (immediately in front of the glacier face) of LeConte Glacier and estimated that 88.7% of the outflow was entrained seawater, 10.8% from subglacial discharge, and only 0.5% from ice melt. Therefore, besides the importance of the feedback between ocean properties and melt rates on the ice face, it is also necessary to focus on how an alteration of the retreat rate of tidewater glaciers and meltwater outflow will affect the adjacent coastal ocean.

One of the first reviews of the oceanographic processes in glacially influenced fjords was done by Syvitski (1989) and later expanded by Powell (1990). They asserted that subglacial discharges take the form of a buoyant jet whose behavior depends mostly on the density difference between the plume (ρ_0) and the ambient fluid

* Corresponding author at: Department of Physics and Physical Oceanography, Memorial University of Newfoundland, St. John's, Canada NL A1B 3X7.
Tel.: +1 709 8642407.

E-mail address: j.salcedo@mun.ca (J. Salcedo-Castro).

(ρ_a), the diameter d of the tunnel opening located at the base or at mid-depth of the glacier face, and the initial jet velocity u_0 , all these variables being represented in the Froude number:

$$Fr = \frac{u_0}{\left(gd \left(\frac{\rho_a - \rho_0}{\rho_0}\right)\right)^{1/2}}, \quad (1)$$

where g is the gravitational acceleration. According to this conceptual model, the initial horizontal jet is directed upward immediately after leaving the tunnel for situations characterized with $|Fr| \sim 0$ (Fig. 1, left). In addition, the influence of the initial momentum depends on the angle (β) between the tangent to the central axis of the jet and the horizontal plane (for $\beta = 0$, initial momentum predominates; for $\beta = 90$, buoyancy predominates). Therefore, circulation in a glacial fjord during the melting season can be summarized as a subglacial buoyant jet producing a buoyant wall plume rising along the ice face; and a horizontal buoyant flow spreading at the surface or mid-depth (Fig. 1, right).

The effect of confined depth on buoyant jets has been the object of many studies. One of the first experimental and theoretical investigations was carried out by Jirka and Harleman (1973) and further studied by others (Jirka, 1982; Jirka and Harleman, 1979; Lee and Jirka, 1981). According to this model, a buoyant jet in confined depth can be schematized into four zones: the buoyant jet; the surface impingement; internal hydraulic jump; and the stratified counterflow. One of the most important results of this model was to establish that the structure and dilution at each zone can be defined as function of only three dimensionless parameters: the Froude number Fr , the relative submergence H/d (where H is the total depth) and the vertical angle of discharge (θ). In this sense, List (1982) has also stated that the vertical motion in turbulent buoyant jets undergoes an increase in momentum with distance along the path as a result of the continuous buoyancy flux at the source.

Jirka and Harleman (1973) also separated stable and unstable jets in function of these three parameters, where a stable jet was defined as not showing re-entrainment and recirculation cells. This dependence of the stability and mixing of a buoyant jets on Fr and H/d in a confined depth has been observed experimentally and modeled in horizontal buoyant jets (Jirka and Harleman, 1973; Jirka, 1982; Sobey et al., 1988) and vertical buoyant jets (Jirka and Harleman, 1979; Lee and Jirka, 1981; Wright et al., 1991; Kuang and Lee, 2001, 2006).

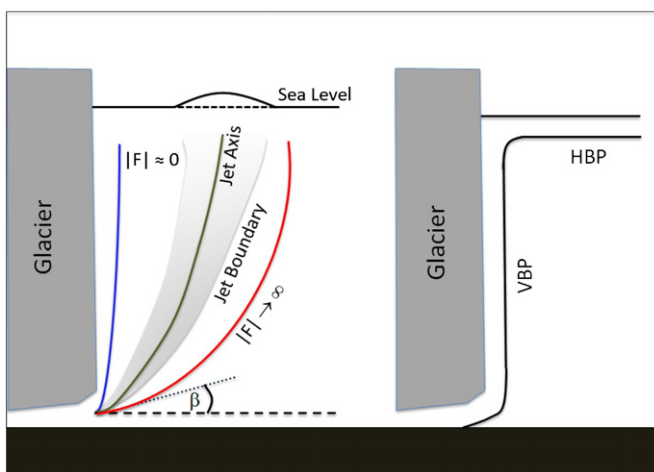


Fig. 1. Left: Proposed scheme of the dependence of subglacial jet circulation on the densimetric Froude number (Fr) (modified from Syvitski, 1989). Right: Different zones defining the structure of a forced plume entering the sea as a plane jet (VBP: Vertical buoyant plume; HBP: Horizontal buoyant plume) (after Powell, 1990).

To date, the response of a glacial fjord to a subglacial freshwater discharge has been studied mostly qualitatively based on simplified theories. Here we expand existing studies by attempting to carry out a fundamental numerical study of the process using a fully non-linear and non-hydrostatic model set in an idealized 2D configuration. These numerical experiments do not include ambient stratification, ocean currents, or any ice processes, as we hope to capture some basic understanding about the flow structure and processes caused only by a subglacial discharge in glacial fjords.

2. Methods

2.1. Model

Compared to fjords in general, glacial fjords present freshwater entering the fjord at depth, either as subglacial or englacial discharges. This causes a narrow rising plume of freshwater with a typical horizontal length scale $L \sim 1$ m, much smaller than the vertical scale of the plume which is roughly the fjord depth, i.e. $H \sim 100$ m. The freshwater forcing in a glacial fjord is therefore highly non-hydrostatic since $H/L \gg 1$ (Marshall et al., 1997). Standard hydrostatic models cannot, therefore, be used to simulate glacial fjords dynamics, unless the rising plume could be parameterized in some way. There is, however, no information for such a parameterization.

In this study, idealized two-dimensional numerical simulations were carried out to understand the plume response to different forcing situations. The model used is a non-hydrostatic, two-dimensional, laterally averaged model (Bourgault and Kelley, 2004). This model uses a finite difference scheme with a variable mesh z -coordinate C -grid and solves the following equations:

$$\frac{\partial u}{\partial t} + u \frac{\partial u}{\partial x} + w \frac{\partial u}{\partial z} = -\frac{1}{\rho_0} \frac{\partial p}{\partial x} + \frac{\partial}{\partial x} \left(v_e \frac{\partial u}{\partial x} \right) + \frac{\partial}{\partial z} \left(v_e \frac{\partial u}{\partial z} \right), \quad (2)$$

$$\frac{\partial w}{\partial t} + u \frac{\partial w}{\partial x} + w \frac{\partial w}{\partial z} = -\frac{1}{\rho_0} \frac{\partial p}{\partial z} - \frac{\rho}{\rho_0} g + \frac{\partial}{\partial x} \left(v_e \frac{\partial w}{\partial x} \right) + \frac{\partial}{\partial z} \left(v_e \frac{\partial w}{\partial z} \right), \quad (3)$$

along with the two-dimensional continuity equation:

$$\frac{\partial u}{\partial x} + \frac{\partial w}{\partial z} = 0, \quad (4)$$

and the advection–diffusion equation for density:

$$\frac{\partial \rho}{\partial t} + u \frac{\partial \rho}{\partial x} + w \frac{\partial \rho}{\partial z} = \frac{\partial}{\partial x} \left(\kappa_e \frac{\partial \rho}{\partial x} \right) + \frac{\partial}{\partial z} \left(\kappa_e \frac{\partial \rho}{\partial z} \right), \quad (5)$$

where $u(x, z, t)$ is the horizontal velocity component; $w(x, z, t)$ is the vertical velocity (positive upward); $p(x, z, t)$ is the pressure; ρ_0 is a constant reference density; $\rho(x, z, t)$ is the density; g is the gravitational acceleration; $v_e(x, z, t)$ and $\kappa_e(x, z, t)$ are the coefficients of eddy viscosity and diffusivity, respectively. Subgrid-scale processes of viscosity and diffusivity are parameterized in the model following Smagorinsky (1963), which is an adaptive scheme depending on the grid spacing and velocity field and uses an adjustable constant of proportionality (Haidvogel and Beckmann, 1999). Note that in Bourgault and Kelley (2004) the longitudinal section can have a variable width, represented by a width term B , whereas Eqs. (3)–(6) are written here for a channel of constant width, i.e. for $B = \text{constant}$.

The numerical experiments are set in a two-dimensional configuration (x, z), a longitudinal section of a glacial fjord, and with freshwater forcing at the glacier face. All the experiments were run with a free surface.

The total length of the numerical domain is 206 km for all simulations with a total depth $H = 100$ m. The numerical grid has a constant vertical resolution of $\Delta z = 1$ m. In the horizontal, the

grid has a resolution of $\Delta x = 1$ m for $0 < x < 100$ m (i.e. the region of interest). For $x > 100$ m the grid size increases linearly to a maximum of $\Delta x = 5000$ m. The domain is long compared to the plume width such that the seaward boundary condition does not influence the results. All simulations reached steady-state in the region $x < 100$ m before the freshwater front reached the seaward boundary.

At the bottom, a bottom shear stress is imposed following

$$v \frac{\partial u}{\partial z} \Big|_{z=-H} = -C_D |u_b| u_b, \quad (6)$$

where u_b is the bottom cell horizontal velocity, and C_D is a drag coefficient given by the law of the wall (Kundu, 1990),

$$C_D = [\kappa / \ln(l/l_0)]^2, \quad (7)$$

where $\kappa = 0.41$ is von Kármán's constant, l is the height above the bottom, and l_0 is the roughness length, here set to $l_0 = 1.0 \times 10^{-3}$ m.

At the seaward open boundary, the horizontal velocity u and density ρ are calculated using the following radiation condition:

$$\frac{\partial u}{\partial t} + u \frac{\partial u}{\partial x} = 0 \quad (8)$$

and

$$\frac{\partial \rho}{\partial t} + u \frac{\partial \rho}{\partial x} = 0, \quad (9)$$

respectively. Note however that these seaward boundary conditions have little practical effect since, as mentioned above, simulations are stopped before the freshwater reaches the seaward boundary.

In all experiments, the glacier is represented as a vertical wall with a no-slip boundary condition. The initial condition is defined as still, uniform density water. The only forcing is a steady flow produced at the open cells set through the glacier face.

2.2. Control parameters

The control parameters of the simulation are: the total depth of the fjord H , the opening depth h , the opening size d , the jet velocity u_0 and the density difference $\Delta \rho = \rho_a - \rho_0$, where ρ_a is the ambient water density (Fig. 2).

Two non-dimensional numbers characterize the experiments. The Reynolds number

$$Re = \frac{u_0 d}{\nu} \quad (10)$$

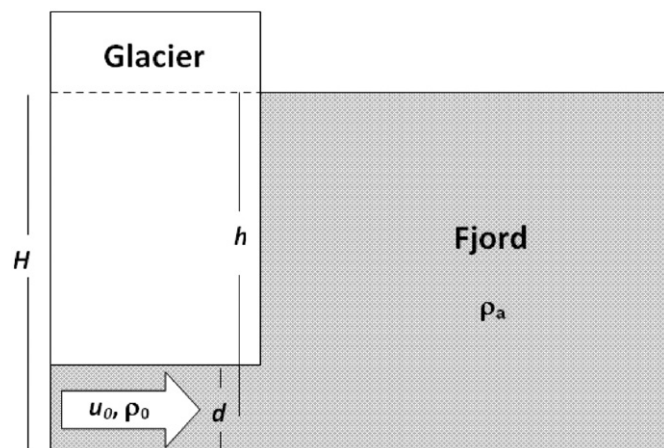


Fig. 2. Schematic representation of a glacial fjord, showing parameters considered in numerical experiments.

Table 1

Control parameters and non-dimensional numbers for experiments of subglacial freshwater discharges.

Run	d (m)	u_0 (m s ⁻¹)	$\Delta \rho$ (kg m ⁻³)	Re	Gr	Fr
1	1	0.01	0.001	1.0×10^4	1.0×10^7	3.2
2	1	0.01	0.010	1.0×10^4	1.0×10^8	1.0
3	1	0.01	0.102	1.0×10^4	1.0×10^9	0.32
4	1	0.01	1.019	1.0×10^4	1.0×10^{10}	0.10
5	1	0.01	10.194	1.0×10^4	1.0×10^{11}	0.030
8	1	0.1	0.102	1.0×10^5	1.0×10^9	3.2
9	1	0.1	1.019	1.0×10^5	1.0×10^{10}	1.0
10	1	0.1	10.194	1.0×10^5	1.0×10^{11}	0.32
11	2	0.05	12.742	1.0×10^5	1.0×10^{12}	0.10
12	4	0.025	15.928	1.0×10^5	1.0×10^{13}	0.030
13	7	0.014	29.719	1.0×10^5	1.0×10^{14}	0.010
18	1	1.0	10.194	1.0×10^6	1.0×10^{11}	3.2
19	2	0.5	12.742	1.0×10^6	1.0×10^{12}	1.0
20	4	0.25	15.928	1.0×10^6	1.0×10^{13}	0.32
21	8	0.125	19.910	1.0×10^6	1.0×10^{14}	0.10

characterizes the momentum flux; and the Grashof number

$$Gr = \frac{(\rho_a - \rho_0) g d^3}{\rho_0 \nu^2} \quad (11)$$

characterizes the buoyancy flux, where $\nu = 1.0 \times 10^{-6}$ m² s⁻¹ is the kinematic viscosity of freshwater.

Although some authors have argued that the trajectory of the buoyant jet will depend on these two numbers (Arakeri et al., 2000; He et al., 2002), Angirasa (1999) suggested that the effects of the buoyancy are important only when jet velocities are small. Another number that determines the relative importance of the jet flow and the buoyancy flow is the Froude number (Eq. (1)), equivalent to the ratio of inertial to buoyancy forces ($Fr = Re/Gr^{1/2}$) (Arakeri et al., 2000). Therefore, there are two limiting cases: when $Re \ll Gr^{1/2}$, corresponding to a buoyancy-dominated flow; and when $Re \gg Gr^{1/2}$, which results in a forced convection jet problem.

Another important parameter that characterizes the geometry of the experiment is the relative submergence, defined as the ratio between the total depth and the width of the opening, i.e.:

$$\delta = \frac{H}{d}. \quad (12)$$

Although the experiments were defined in terms of the Re–Gr space, the relative submergence and the depth of the opening h change in different runs as a consequence of varying the opening size d .

A number of experiments covering a range of buoyancy and jet-dominated conditions in a glacial fjord were run. The experiments encompass a range of Re between 10^4 and 10^6 whereas Gr number ranges from 10^7 to 10^{14} . The parameter space was set within constraints imposed by the grid size and according to ranges approximately realistic of jet velocity and density differences. For instance, for jet velocities ranging between 0.05 and 2 m s⁻¹ and densities differences ranging between 24 and 28 kg m⁻³ (corresponding to salinities between 30 to 34) Fr varies between 0.02 and 3.8. These experiments are summarized in Table 1.

3. Results

After issuing horizontally from the tunnel, the jet turns into a vertical plume rising along the glacier face and, after impinging the surface, the plume spreads horizontally and thickens progressively as it moves seaward. This pattern is similar in jet-dominated conditions (i.e. $Re \gg Gr^{1/2}$, Fig. 3) and buoyancy-dominated conditions (i.e. $Re \ll Gr^{1/2}$, Fig. 4). Jet-dominated conditions take

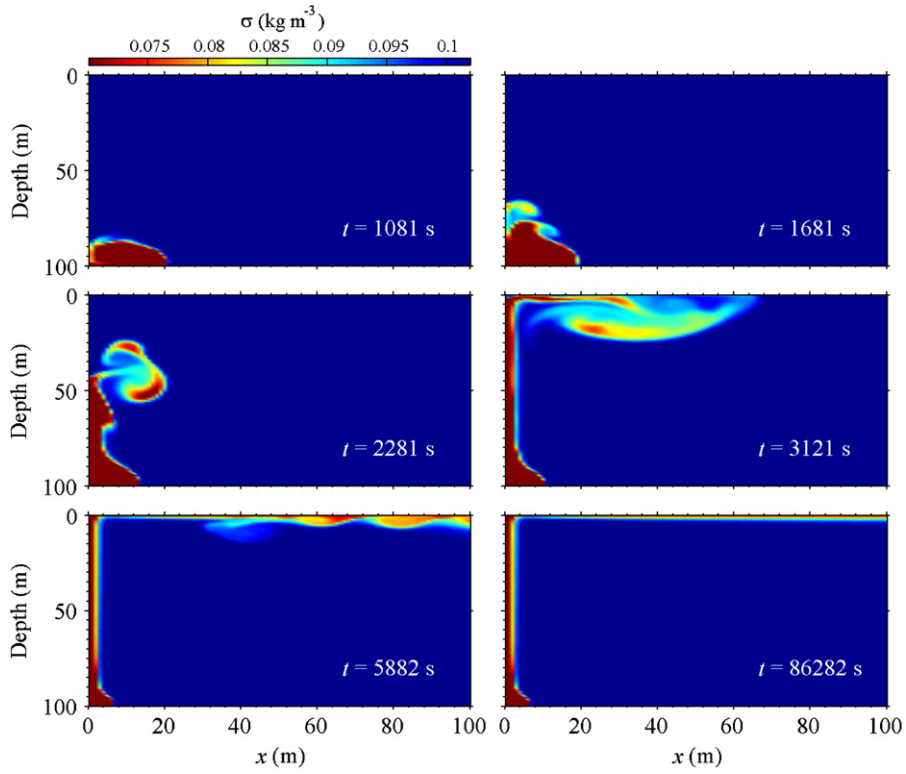


Fig. 3. Sequence of density anomaly representing the rising (vertical) plume and spreading of the surface plume observed in a typical jet-dominated experiment (run # 8, $Fr=3.16$).

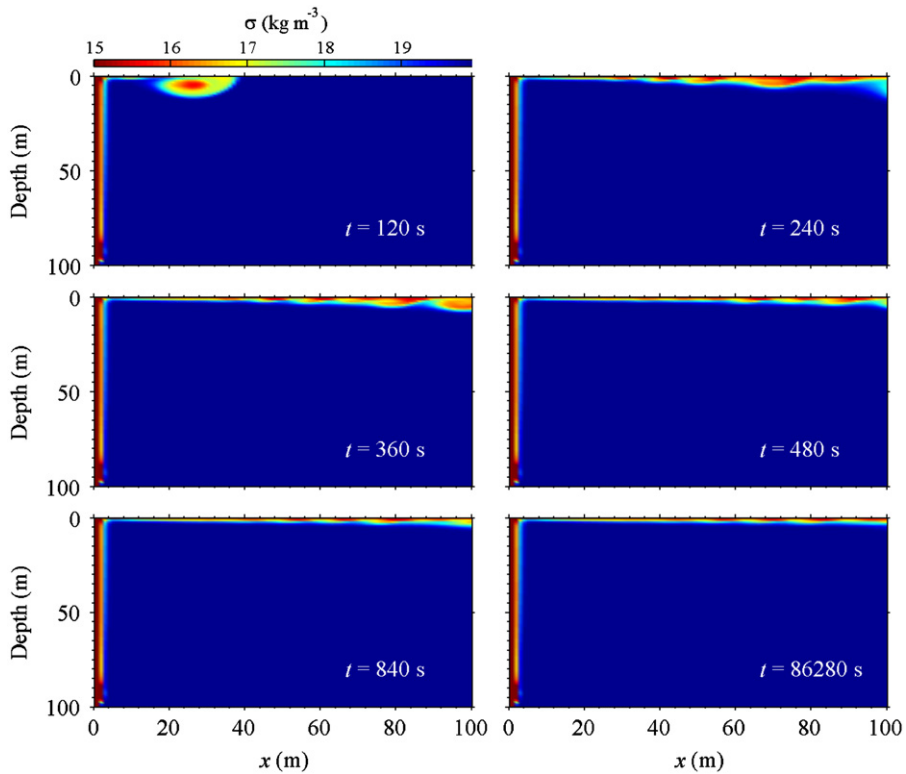


Fig. 4. Sequence of density anomaly representing the rising (vertical) plume and spreading of the surface plume observed in a typical buoyancy-dominated experiment (run # 21, $Fr=0.1$).

longer to reach steady-state and exhibit a bulb-shaped structure where the issuing jet protrudes horizontally along the bottom before detaching and rising along the wall (Fig. 3).

At steady-state, the structure observed in all experiments consists of a horizontal wall jet at the bottom, a plume along the glacier face, a surface bulging region and a horizontal surface

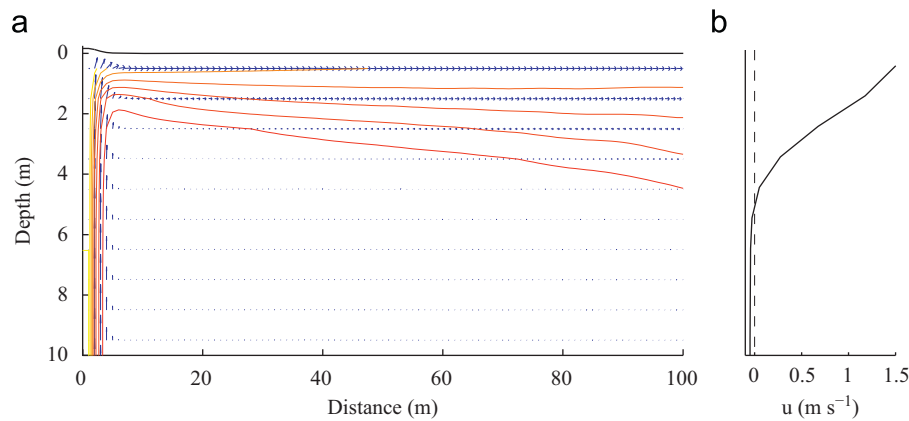


Fig. 5. (a) Structure of density (1 kg m^{-3} between contour lines) and velocity (largest arrows representing 1.8 m/s) and (b) horizontal velocity profile showing a typical estuarine circulation developed in a run buoyancy-dominated (run # 21, $Fr=0.1$). For clarity, only the first 10 meters are shown but the simulated fjord is 100 m deep.

plume. The surface bulging region is where an uplift of the free surface is produced by the rising vertical plume and a transition to horizontal plume is observed (Fig. 5). The limit between this region and the horizontal surface plume is marked by the point where the upper layer is thinnest. The horizontal circulation is estuarine-like (Fig. 5), with a thin ($\sim 5 \text{ m}$ thick) upper layer moving seaward and a deep lower layer moving toward the glacier (Fig. 5).

3.1. Horizontal velocity

The structure of the horizontal velocity at the surface u_p exhibits two regions (as shown in Fig. 6). The first region, immediately following the surface impingement caused by the vertical plume, represents a transitional zone with a sharp linear increase in velocity along the surface. The second region is a decelerating zone, where the plume velocity gradually decreases.

For the transition region, a linear fit was constructed between velocity and distance (non-dimensionalized as $u_p u_0^{-1}$ and xd^{-1} , respectively). The slope b (representing the rate of velocity increase as a function of offshore distance in each experiment) was plotted as a function of Fr as shown in Fig. 7(a). It can be seen that the velocity increase is higher in buoyancy-dominated experiments (low Fr number) and decreases as the experiments become jet-dominated (high Fr number).

On the other hand, for the decreasing stretch a logarithmic fit of the form

$$y = \ln(ax^b) \quad (13)$$

was adjusted between non-dimensionalized velocity and distance; where b represents how quickly u_p changes as a function of distance from the tunnel (b positive represents an increase whereas a negative value represents a decrease). The slope b was plotted as function of Fr and the resultant relationship is shown in Fig. 7(b). In this case a negative sign was added to the slope to enable the logarithmic fit. Similar to what was observed in the transitional region, the rate of velocity decrease is higher in buoyancy-dominated experiments and slower for jet-dominated experiments.

3.2. Dilution factor

In order to evaluate the degree of mixing along the horizontal plume a dilution factor was defined as

$$S = \frac{\rho_a - \rho_0}{\rho_a - \rho_p} \quad (14)$$

where ρ_p is the plume density, which correspond to the values closest to the surface. These definitions are commonly used in the

analysis of plume dilution (Anwar, 1973; Lee and Lee, 1998), and buoyant jets dilution (Chen and Rodi, 1980; Huai et al., 2010). Similar to horizontal velocity, dilution along the surface exhibits two patterns. The first region (transitional zone) shows a linear dilution rate along a short stretch which is followed by a region with a slower dilution rate (Fig. 6). A linear fit was applied to the zone nearest to the glacier face. The corresponding slope (representing the rate of dilution increase as a function of distance for each experiment) was related to Fr according to the expression shown in Fig. 8. On the other hand, a logarithmic fit (Eq. (13)) was computed for the slow dilution stretch, and its slope was related to Fr in a similar way (Fig. 8). In this last case it was necessary to add the H/d ratio to this expression to account for differences in relative submergence between experiments. Buoyancy-dominated experiments (low Fr number) have a higher dilution rate along the transitional stretch in comparison with jet-dominated experiments (high Fr number). A similar pattern is observed when comparing the dilution rate along the slow increasing stretch.

3.3. Estuarine circulation

The response of the estuarine circulation is now assessed by examining the relationship between the surface velocity (normalized by u_0) and dilution factor S and the Froude number at distance $10d$ from the glacier face. Similar to the rate of velocity decrease (Fig. 7(b)), the velocity of the surface layer is related to Fr according to a negative power function (Fig. 9(a)), implying that the estuarine circulation is mostly driven by the buoyancy flux from the source (subglacial jet issuing at the bottom). As expected, the plume dilution is also higher at lower Fr (Fig. 9(b)), showing a higher entrainment caused by faster velocities at the surface layer.

The presence of a surface layer with higher velocity and dilution produces a stratified shear flow whose opposite effects of stratification and velocity shear can be characterized in terms of the gradient Richardson number (Thorpe, 1968):

$$Ri = -\frac{g}{\rho} \frac{\partial \rho / \partial z}{(\partial u / \partial z)^2} \quad (15)$$

Similar to the plume velocity and dilution factor, Ri was computed at $10d$ away from the glacier and Ri profiles for the 15 experiments are shown in Fig. 10.

For all experiments the interface was located at 2 m depth, where maximum values of buoyancy frequency and velocity shear occurred (see Eq. (15)). The results suggest that Ri is independent of the characteristics of the buoyant jet, since $Ri < 1/4$ (average $Ri = 0.040 \pm 0.005$) at the interface in all the experiments (Fig. 10).

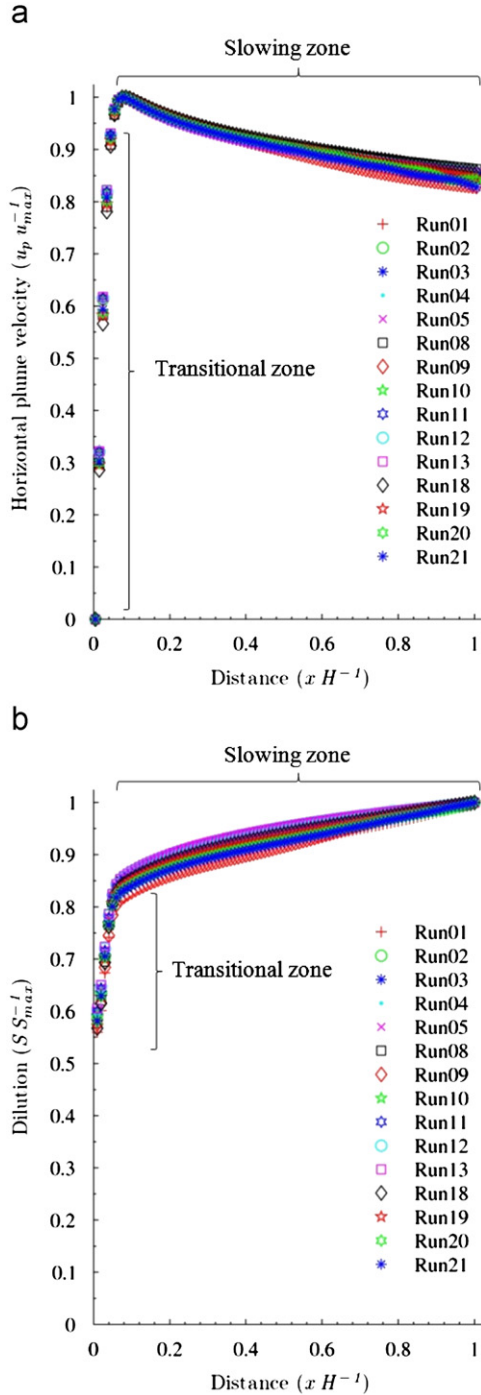


Fig. 6. (a) Horizontal variation of plume velocity as function of distance from the glacier. (b) Horizontal variation of plume dilution as function of distance from the glacier. Velocity, dilution and horizontal distance were non-dimensionalized with u_{max} , S_{max} and H , respectively.

This is confirmed by plotting the minimum Ri values at the interface as a function of Fr (Fig. 10). Despite favorable conditions for shear instability ($Ri < 1/4$), some experiments (five of 15 experiments) did not show instabilities at steady-state (Fig. 11), presumably because the instabilities are damped by the Smagorinsky scheme for those cases. All other experiments show a continuous growth and decay of shear instabilities at steady-state (see for example Figs. 4 and 12).

Another way to assess the fjord's response is by comparing the buoyancy flux at the tunnel opening with the intensity of the

estuarine circulation. The buoyancy flux (B_0 , $m^3 s^{-3}$) was computed at the mouth of the tunnel as

$$B_0 = \frac{g d u_0 (\rho_a - \rho_0)}{\rho_a} \quad (16)$$

The intensity of the estuarine circulation was estimated as the vertically integrated kinetic energy density (K_r , $J m^{-2}$), computed at a distance $10 d$ away from the glacier according to

$$K_r = \frac{1}{2} \int_{-H}^{\eta} \rho (u^2 + w^2) dz \quad (17)$$

The estuarine circulation (K_r) intensifies as the buoyancy flux (B_0) gets higher (Fig. 13). This is consistent with the results for the surface velocity and dilution since a higher buoyancy flux intensifies the estuarine circulation.

The fjord's response can also be assessed by examining how the water column stratification is modified by the freshwater forcing. This is done here by computing the potential energy anomaly (PEA), defined as the equivalent work to homogenize the water column (Simpson et al., 1978; O'Donnell, 2010), (ϕ , $J m^{-2}$), which is expressed as

$$\phi = \int_{-H}^{\eta} g (\rho - \bar{\rho}) z dz, \quad (18)$$

where $\bar{\rho}$ represents the depth-averaged density:

$$\bar{\rho} = \frac{1}{H} \int_{-H}^{\eta} \rho(z) dz. \quad (19)$$

Similar to K_r , the PEA was computed at a distance equivalent to $10 d$ away from the glacier and showed an increase with the buoyancy flux (B_0) (Fig. 14).

These results of vertically integrated kinetic energy density (K_r) and potential energy anomaly (ϕ) can be related to the total energy input at the source which is represented as the sum of the kinetic energy (KE , $J m^{-2}$)

$$KE = \frac{1}{2} u_0^2 d \rho_0, \quad (20)$$

and the available potential energy (APE , $J m^{-2}$)

$$APE = g dh \Delta \rho. \quad (21)$$

It can be seen that the ratio $K_r / (KE + APE)$ (Fig. 15) and the ratio $\phi / (KE + APE)$ (Fig. 15) are similarly related to the Froude number at the source, with an increasing trend as Fr increases. This result shows that buoyancy-dominated flows exhibit an estuarine circulation whose energy is very small compared to the total energy influx at the source, and that this proportion increases as Fr increases.

4. Discussion

Once steady-state is reached, the structure observed in all the experiments consists of a zone of the wall jet at the bottom, a rising plume along the glacier face and a horizontal surface plume region producing an estuarine circulation. Also, in this last region it was possible to distinguish two zones: a short transition zone with a rapid increase in velocity and dilution, and a larger zone showing a slow decrease in velocity and increase in dilution (Fig. 16). These structures have been observed in other numerical and experimental studies of vertical (Jirka and Harleman, 1979; Wright et al., 1991; Kuang and Lee, 2006) and horizontal forced plumes (Jirka and Harleman, 1973; Jirka, 1982). The increase in velocity observed in the transitional zone was caused by the higher pressure gradient caused by the surface elevation when the wall plume reaches the surface. The velocity in the transition zone depends on the source buoyancy as shown by the relationship between velocity and Fr number in this zone.

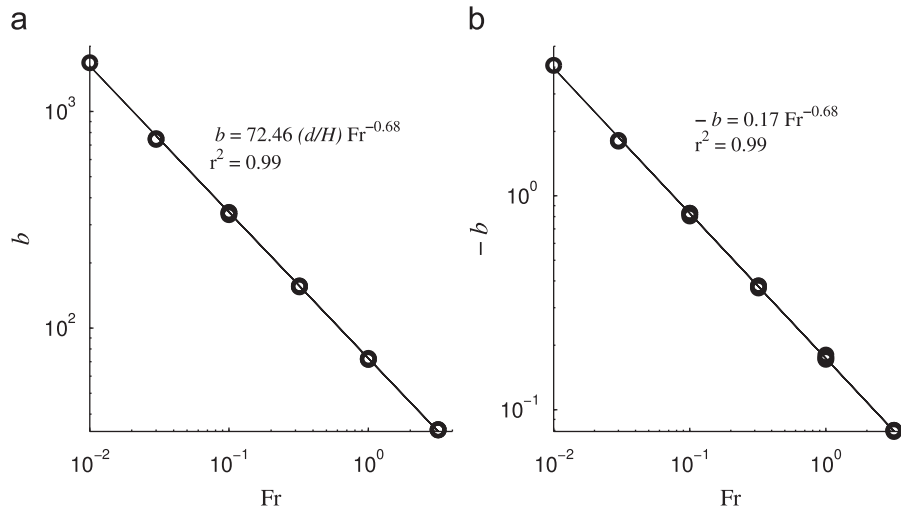


Fig. 7. (a) Rate of velocity increases (linear fit) as function of distance along the increasing (transitional) stretch plotted as function of Fr. (b) Same plot corresponding to the decreasing stretch (Note negative sign added to make possible the log fit).

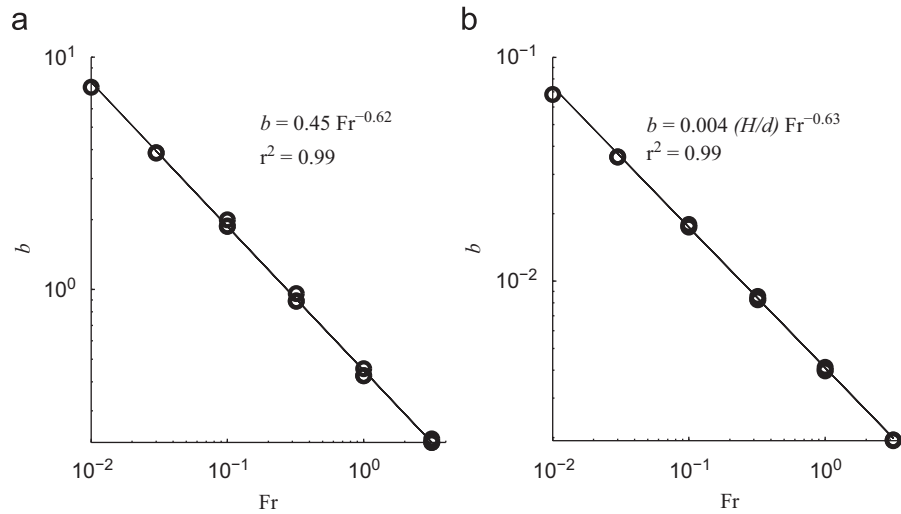


Fig. 8. (a) Rate of dilution increases as function of distance along the fast increasing (transitional) stretch plotted as function of Fr. (b) Same plot corresponding to the slow increasing stretch.

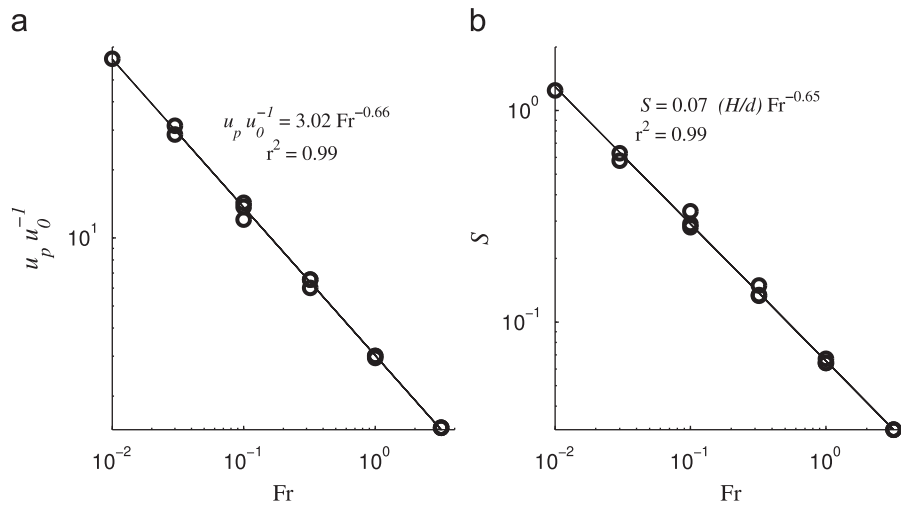


Fig. 9. Variation of plume velocity (a) and plume dilution (b) as a function of Fr at a distance equivalent to $10 d$, where d is the opening diameter.

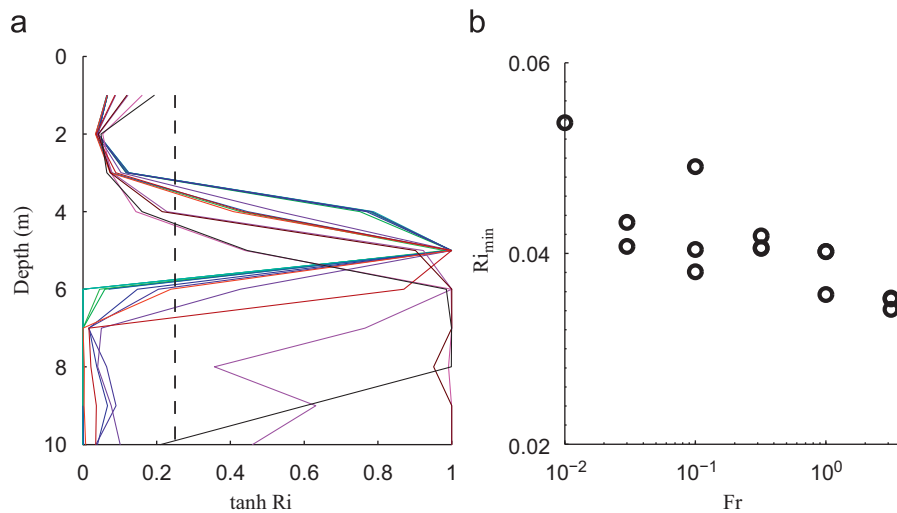


Fig. 10. (a) Profiles of gradient Ri number in the top 10 m of the water column (dashed line shows $Ri=0.25$) and (b) plot of minimum Ri_{min} at the sheared interface as function of Fr number at a distance equivalent to $10 d$, where d is the opening diameter.

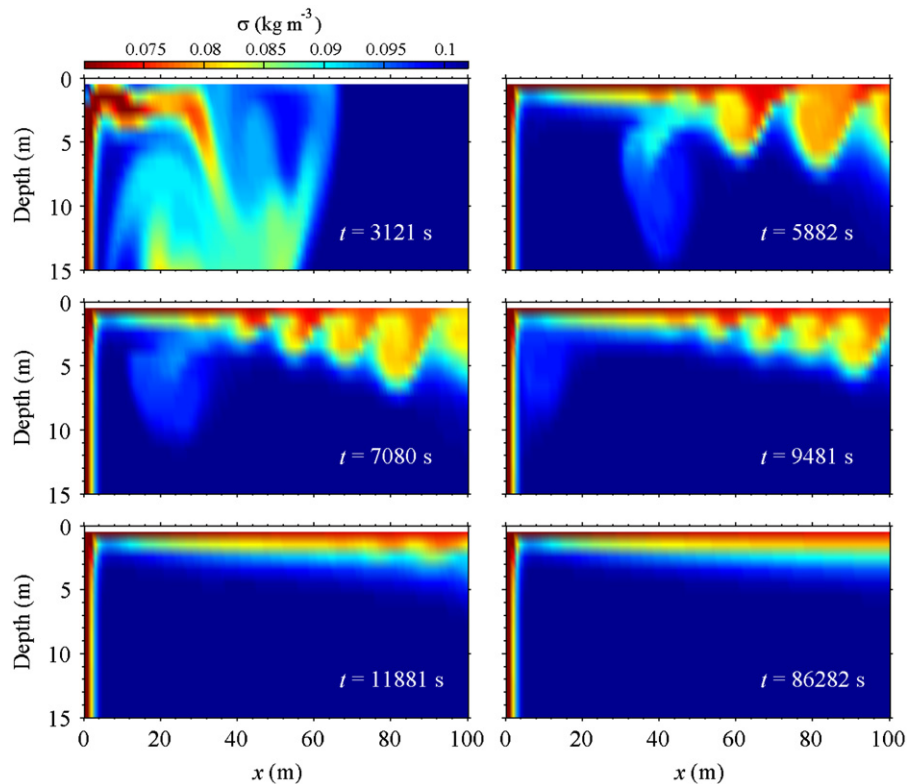


Fig. 11. Sequence of density anomaly representing rising (vertical) plume and spreading of surface plume observed in a typical jet-dominated experiment (run08, $Fr=3.16$).

The momentum-dominated discharge issuing at the foot of the glacier is a wall jet whose momentum is rapidly lost due to friction with the bottom. In this sense, Powell (1990) mentioned that friction contributes to changing effectively jet-dominated flows to plume-like flows. This process is not observed in buoyancy-dominated discharges due to a combination of small Fr number and a high submergence ratio that make the flow to rise immediately after leaving the tunnel (Sobey et al., 1988).

From some experimental work on buoyant jets (Jirka and Harleman, 1979; Wright et al., 1991), it is known that Fr can reach values up to 2 orders of magnitude higher than our highest

value. Considering this wider range, we can assert that the structures observed in our results correspond to what Syvitski's conceptual model refers as " $Fr \sim 0$ ". However, we propose that Syvitski's conceptual model can be complemented by also considering the relative submergence, H/d . According to the model proposed by Jirka and Harleman (1973) and Jirka (1982), the structure of buoyant discharges in finite depths is related to Fr and H/d (also dependent on jet discharge angle). These two parameters are also the base for the criterion of the discharges stability. Therefore, according to this criterion, subglacial buoyant jets can be described as a type of *stable* buoyant discharges, as they are observed to

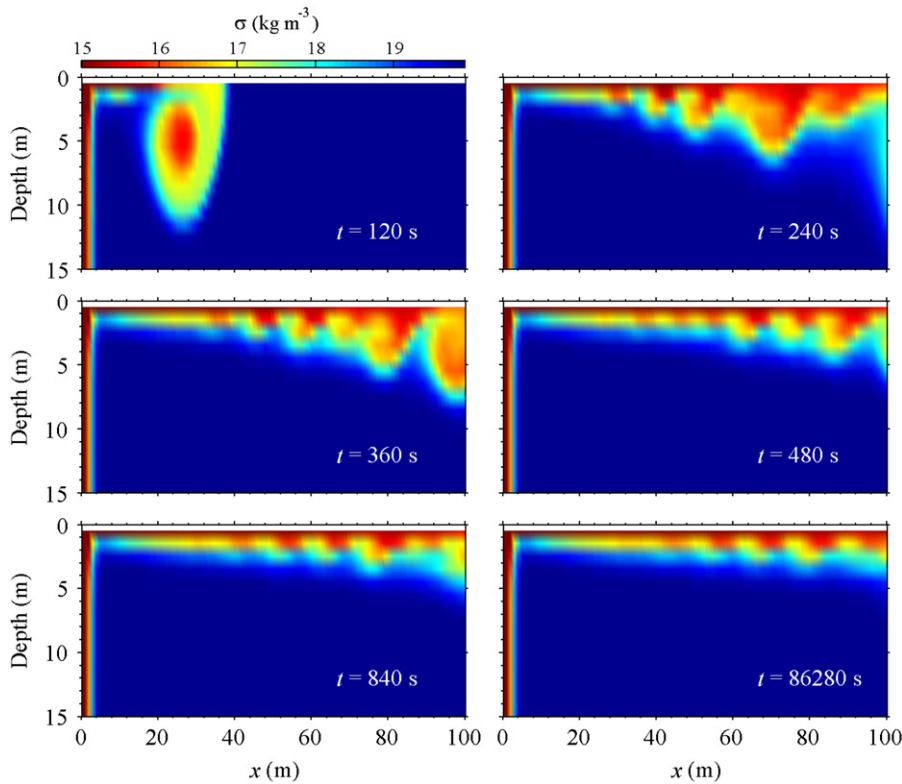


Fig. 12. Sequence of density anomaly representing rising (vertical) plume and spreading of surface plume observed in a typical buoyancy-dominated experiment (run21, Fr=0.1).

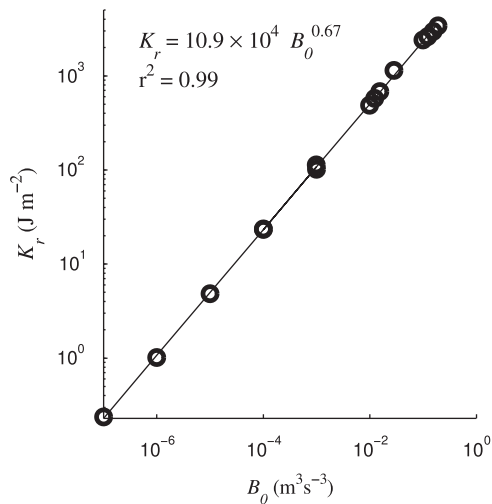


Fig. 13. Relationship between the buoyancy flux B_0 and the intensity of estuarine circulation, computed as K_r , at a distance equivalent to $10 d$, where d is the opening diameter.

remain attached to the glacier face and do not show recirculation cells up to the surface (Fig. 16).

The Richardson number at the sheared estuarine interface is $< 1/4$ in all the experiments within the first 100 m away from the glacier. The limits and instability of this region are similar to the zone of internal hydraulic jump described in confined buoyant jets by Jirka and Harleman (1973), which exhibits high entrainment rates (Jirka and Harleman, 1979; Wright et al., 1991; Kuang and Lee, 2006) and extends for a horizontal distance equal or greater than $2.5H$. This condition suggests that the estuarine circulation is dynamically unstable in the near-field (first 100 m

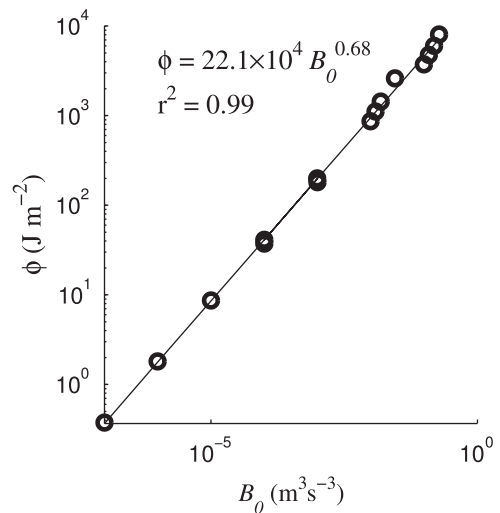


Fig. 14. Relationship between the buoyancy flux B_0 and the potential energy anomaly ϕ , at a distance equivalent to $10 d$, where d is the opening diameter.

away from the glacier), independently of the forcing conditions, over the parameter space explored here. It is worth mentioning that, in some simulations, the growing of the instabilities could have been prevented by the Smagorinsky subgrid scale model as the eddy diffusivity is increased and instabilities may be inhibited when the shear is stronger than buoyancy (see Eq. (25) in Bourgault and Kelley, 2004).

These results show that a small part of the total energy input is converted into estuarine circulation in buoyancy-dominated cases whereas this conversion is higher in jet-dominated experiments. In general, stratification and estuarine circulation depend primarily on

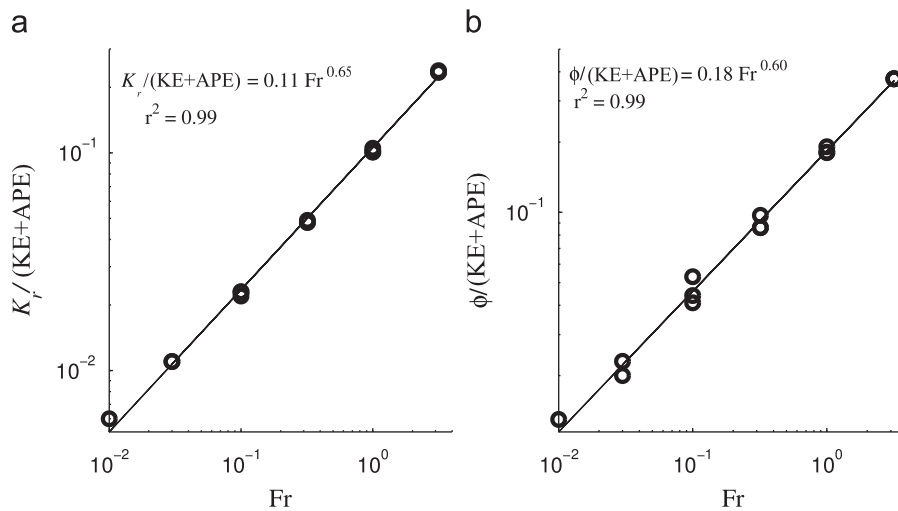


Fig. 15. Variation of $K_r/(KE+APE)$ (a) and the ratio $\phi/(KE+APE)$ (b) as function of Fr at a distance equivalent to $10d$, where d is the opening diameter.

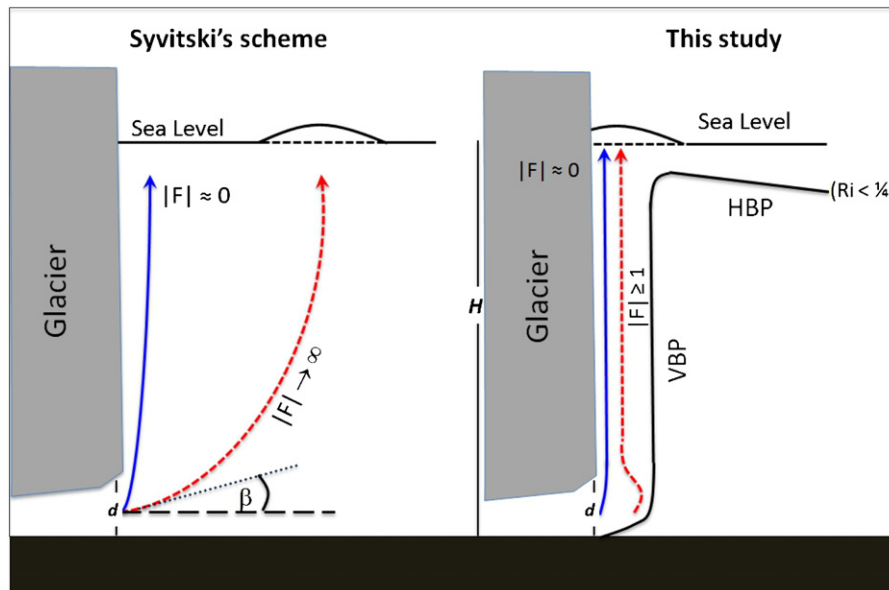


Fig. 16. Comparison of schemes representing a subglacial discharge. Left: Syvitski (1989) scheme, proposing dependence on Fr only. Right: This study, proposing dependence on Fr and H/d (VBP: Vertical buoyant plume; HBP: Horizontal buoyant plume).

the buoyancy flux and available potential energy since kinetic energy at the source is relatively smaller and jet momentum is rapidly lost when the jet is issuing from the tunnel. This pattern is characteristic of buoyant jets (Fischer et al., 1979; Powell, 1990).

The nature of the jet at the bottom of the glacier is difficult to observe in nature. In this sense, the quantitative relationships found in this study may be used to obtain an estimate of the characteristics of the subglacial freshwater fluxes from observed far-field density and velocity observations.

Since this investigation considered a simplified scenario, a further step should explore the effect of other variables such as stratification and tides. Another possibility would be simulate pulse-like discharges and include ice wall melting to represent more realistically the behavior of these discharges.

5. Summary and conclusion

Circulation associated with subglacial freshwater discharge issuing in a glacial fjord is characterized by a combination of a

wall jet, a vertical buoyant plume, and a surface plume giving place to an estuarine circulation. There is a transition zone caused by the surface elevation caused by the vertical buoyant plume, where rapid increases of velocity and dilution were observed. The characteristics of the estuarine circulation are related to the Froude number and they are also influenced by the relative submergence H/d . Buoyancy-dominated discharges showed a more rapid change of velocity and dilution in comparison with jet-dominated discharges.

The structure of the vertical buoyant plume agrees with the model proposed by Syvitski (1989) since the plume remains attached to the wall (glacier face) for the low Fr magnitudes set in the experiments. However, as the circulation is determined by a buoyant jet in confined depth, the relative submergence H/d is an important parameter to be included. We propose a new schematic diagram for the circulation in glacial fjord, shown in Fig. 16.

Buoyancy flux is the most important forcing in subglacial plumes as jet momentum is rapidly lost and processes like mixing, estuarine circulation and stratification are mainly related to the buoyancy flux and the available potential energy.

Acknowledgements

This research was carried out through the Circumpolar Flaw Lead (CFL) System Study and funded by the Canadian International Polar Year (IPY) program office and the Natural Sciences and Engineering Research Council (NSERC). We also thank the reviewers for their helpful suggestions for improving the manuscript.

References

- Angirasa, D., 1999. Interaction of low-velocity plane jets with buoyant convection adjacent to heated vertical surfaces. *Numerical Heat Transfer, Part A* 35, 67–84.
- Anwar, H.O., 1973. Two-dimensional buoyant jet in a current. *Journal of Engineering Mathematics* 7 (4), 297–311.
- Arakeri, J., Das, D., Srinivasan, J., 2000. Bifurcation in a buoyant horizontal laminar jet. *Journal of Fluid Mechanics* 412, 61–73.
- Bourgault, D., Kelley, D.E., 2004. A laterally averaged nonhydrostatic ocean model. *Journal of Atmospheric and Oceanic Technology* 21, 1910–1924.
- Chen, C.J., Rodi, W., 1980. *Vertical Turbulent Buoyant Jets—A Review of Experimental Data*. Pergamon Press.
- Cowan, E.A., 1992. Meltwater and tidal currents: controls on circulation in a small glacial fjord. *Estuarine, Coastal and Shelf Science* 34, 381–392.
- Fischer, H., List, E.J., Koh, R.C.Y., Imberger, J., Brooks, N.H., 1979. *Mixing in Inland and Coastal Waters*. Academic Press.
- Haidvogel, D.B., Beckmann, A., 1999. *Numerical Ocean Circulation Modeling*. Imperial College Press.
- He, S., Xu, Z., Jackson, J., 2002. An experimental investigation of buoyancy-opposed wall jet flow. *International Journal of Heat and Fluid Flow* 23, 487–496.
- Horne, E.P.W., 1985. Ice-induced vertical circulation in an Arctic fjord. *Journal of Geophysical Research* 90, 1078–1086.
- Huai, W., Li, Z., Qian, Z., Zeng, Y., Han, J., 2010. Numerical simulation of horizontal buoyant wall jet. *Journal of Hydrodynamics* 22, 58–65.
- Jirka, G.H., 1982. Turbulent buoyant jets in shallow fluid layers. In: Rodi, W. (Ed.), *Turbulent Buoyant Jets and Plumes*. Pergamon Press, pp. 69–120.
- Jirka, G.H., Harleman, D.R.F., 1973. The mechanics of submerged multipoint diffusers for buoyant discharges in shallow waters. Technical Report 169, Ralph M. Parsons Laboratory for Water Resources and Hydrodynamics, Massachusetts Institute of Technology, Cambridge, Massachusetts.
- Jirka, G.H., Harleman, D.R.F., 1979. Stability and mixing of a vertical plane buoyant jet in confined depth. *Journal of Fluid Mechanics* 94, 275–304.
- Josberger, E.G., 1978. A laboratory and field study of iceberg deterioration. In: Husseiny, A.A. (Ed.), *Iceberg Utilization. Proceedings of the First International Conference*, Ames, Iowa, 1977. Pergamon Press, pp. 245–264.
- Josberger, E.G., Martin, S., 1981. A laboratory and theoretical study of the boundary layer adjacent to a vertical melting ice wall in salt water. *Journal of Fluid Mechanics* 111, 439–473.
- Josberger, E.G., Neshyba, S., 1980. Iceberg melt-driven convection inferred from field measurements of temperature. *Annals of Glaciology* 1, 113–117.
- Kuang, C.P., Lee, J.H.W., 2001. Effect of downstream control on stability and mixing of a vertical plane buoyant jet in confined depth. *Journal of Hydraulic Research* 39, 375–391.
- Kuang, C.P., Lee, J.H.W., 2006. Stability and mixing of a vertical axisymmetric buoyant jet in shallow water. *Environmental Fluid Mechanics* 6, 153–180.
- Kundu, P.K., 1990. *Fluid Mechanics*. Academic Press.
- Lee, J.H.W., Jirka, G.H., 1981. Vertical round buoyant jet in shallow depth. *Journal of the Hydraulics Division, ASCE* 107, 1651–1675.
- Lee, W.T., Lee, J.H.W., 1998. Effect of lateral confinement on initial dilution of vertical round buoyant jet. *Journal of Hydraulic Engineering* 124, 263–279.
- List, E.J., 1982. Turbulent jets and plumes. *Annual Review in Fluid Mechanics* 14, 189–212.
- Mackiewicz, N.E., Powell, R.D., Carlson, P.R., Molnia, B.F., 1984. Interlaminated ice-proximal glacial marine sediments in Muir Inlet, Alaska. *Marine Geology* 57, 113–147.
- Marshall, J., Hill, C., Perelman, L., Adcroft, A., 1997. Hydrostatic, quasi-hydrostatic, and nonhydrostatic ocean modeling. *Journal of Geophysical Research* 102 (C3), 5733–5752.
- Matthews, J., Quinlan, A., 1975. Seasonal characteristics of water masses in Muir Inlet, a fjord with tidewater glaciers. *Journal of the Fisheries Research Board of Canada* 32, 1693–1703.
- Motyka, R.J., Hunter, L., Echelmeyer, K.A., Connor, C., 2003. Submarine melting at the terminus of a temperate tidewater glacier, LeConte Glacier, Alaska, USA. *Annals of Glaciology* 36, 57–65.
- Neshyba, S., 1977. Upwelling by icebergs. *Nature* 267 (5611), 507–508.
- Neshyba, S., Josberger, E.G., 1980. On the estimation of Antarctic iceberg melt rate. *Journal of Physical Oceanography* 10, 1681–1685.
- O'Donnell, J., 2010. The dynamics of estuary plumes and fronts. In: Valle-Levinson, A. (Ed.), *Contemporary Issues in Estuarine Physics*. Cambridge University Press, pp. 186–246.
- Peizhen, Z., Molnar, P., Downs, W.R., 2001. Increased sedimentation rates and grain sizes 2–3 Myr ago due to the influence of climate change on erosion rates. *Nature* 410, 891–897.
- Powell, R.D., 1990. Glacial marine processes at grounding-line fans and their growth to ice-contact deltas. In: Dowdeswell, J.A., Scourse, J.D. (Eds.), *Glacial Marine Environments: Processes and Sediments*, vol. 53. Geological Society Special Publication, pp. 53–73.
- Simpson, J.H., Allen, C.M., Morris, N.C.G., 1978. Fronts on the continental shelf. *Journal of Geophysical Research* 83, 4607–4614.
- Smagorinsky, J., 1963. General circulation experiments with primitive equations. I. The basic experiment. *Monthly Weather Review* 91, 99–164.
- Sobey, R.J., Johnston, A.J., Keane, R.D., 1988. Horizontal round buoyant jet in shallow water. *Journal of Hydraulic Engineering* 114 (8), 910–929.
- Solomon, S., Qin, D., Manning, M., Chen, Z., Marquis, M., Averyt, K.B., Tignor, M., Miller, H.L. (Eds.), 2007. *Contribution of Working Group I to the Fourth Assessment Report of the Intergovernmental Panel on Climate Change*. Cambridge University Press.
- Svendsen, H., Beszczynska-Møller, A., Hagen, J.O., Lefauconnier, B., Tverberg, V., Gerland, S., Børre-Orbæk, J., Bischof, K., Papucci, C., Zajaczkowski, M., Azzolini, R., Bruland, O., Wiencke, C., Winther, J.G., Dallmann, W., 2002. The physical environment of Kongsfjorden–Krossfjorden, an Arctic fjord system in Svalbard. *Polar Research* 21, 133–166.
- Syvitski, J.P.M., 1989. On the deposition of sediment within glacier-influenced fjords: oceanographic controls. *Marine Geology* 85, 301–329.
- Thorpe, S.A., 1968. A method of producing a shear flow in a stratified fluid. *Journal of Fluid Mechanics* 32, 693–704.
- Walters, R.A., Josberger, E.G., Driedger, C.L., 1988. Columbia Bay, Alaska: An 'upside down' estuary. *Estuarine, Coastal and Shelf Science* 26, 607–617.
- Wright, S.J., Roberts, P.J.W., Zhongmin, Y., Bradley, N.E., 1991. Surface dilution of round submerged buoyant jets. *Journal of Hydraulic Research* 29, 67–89.